Two-Dimensional Structure of β-Amyloid(10−35) Fibrils†

Tammie L. S. Benzinger,‡ David M. Gregory,§,|| Timothy S. Burkoth,⊥ Hélène Miller-Auer,‡ David G. Lynn,⊥ Robert E. Botto,|| and Stephen C. Meredith*,‡

Department of Pathology and Department of Chemistry, The University of Chicago, Chicago, Illinois 60637, and Chemistry Division, Argonne National Laboratory, Argonne, Illinois 60439

Received July 2, 1999; Revised Manuscript Received November 9, 1999

ABSTRACT: β-Amyloid (Aβ) peptides are the main protein component of the pathognomonic plaques found in the brains of patients with Alzheimer's disease. These heterogeneous peptides adopt a highly organized fibril structure both in vivo and in vitro. Here we use solid-state NMR on stable, homogeneous fibrils of A$\beta_{(10-35)}$. Specific interpeptide distance constraints are determined with dipolar recoupling NMR on fibrils prepared from a series of singly labeled peptides containing ^{13}C-carbonyl-enriched amino acids, and skipping no more that three residues in the sequence. From these studies, we demonstrate that the peptide adopts the structure of an extended parallel β-sheet in-register at pH 7.4. Analysis of DRAWS data indicates interstrand distances of 5.3 ± 0.3 Å (mean ± standard deviation) throughout the entire length of the peptide, which is compatible only with a parallel β-strand in-register. Intrastrand NMR constraints, obtained from peptides containing labels at two adjacent amino acids, confirm the secondary structural findings obtained using DRAWS. Using peptides with ^{13}C incorporated at the carbonyl position of adjacent amino acids, structural transitions from α-helix to β-sheet were observed at residues 19 and 20, but using similar techniques, no evidence for a turn could be found in the putative turn region comprising residues 25−29. Implications of this extended parallel organization for A$\beta_{(10-35)}$ for overall fibril formation, stability, and morphology based upon specific amino acid contacts are discussed.

β-Amyloid (Aβ)[1] peptides are the main protein component of the pathognomonic plaques found in the brains of patients with Alzheimer's disease. These heterogeneous, neurotoxic peptides, mainly 39−42 amino acids long, are derived from partial proteolysis of the larger transmembrane protein, the β-amyloid precursor protein (βAPP, *1*−*5*), and are widely believed to play a pathogenic role in Alzheimer's disease. In plaques, Aβ peptides are found in highly ordered, but noncrystalline fibrils of a characteristic morphology on electron microscopy (*6*−*16*). In a previous study, we have reported that the hydrophobic core region of A$\beta_{(10-35)}$—residues 15 through 18—exists in a parallel β-sheet with like residues directly aligned along the strand, i.e., "in-register" (*17, 18*). This conclusion was derived from solid-state NMR measurements of interatomic distances between like atoms in adjacent strands. A parallel β-sheet in-register, if extended throughout the entire length of A$\beta_{(10-35)}$, would constitute a type of "two-dimensional" sheet structure, i.e., a lamina of the full thickness fibril.

Highly ordered yet noncrystalline structures such as β-amyloid are sometimes referred to as paracrystalline, a term used to describe other fibril-forming proteins such as collagen, hemoglobin S, actin, and tropomyosin, as well as viral particles and cell surface structures and intracellular inclusion bodies (*19*−*33*). The structures of self-associating macromolecules which form paracrystalline aggregates pose severe assignment limitations not only because of size and, in some cases, low solubility, but also because of inherent symmetry of the complexes. Amyloids in general are prototypical of paracrystalline materials, but among them, the β-amyloid (Aβ) peptides of Alzheimer's disease are the most tractable at least in terms of the small size of the aggregating peptide. In this paper, we extend the strategy adopted in our previous studies to determine the overall secondary structure and dynamics of the entire peptide within the fibril.

In the present paper and previous studies (*17, 18, 46*), the use of a truncated peptide allowed for the level of reproducibility, stability, and homogeneity of fibril morphology necessary for high-resolution structural studies. The particular truncated peptide was chosen for its biological relevance: (1) Truncated peptides used as models form fibrils of clear morphological similarity to those formed by full-length Aβ

† We thank the Argonne National Laboratory (D.G.L., S.C.M.), the Alzheimer's Association (IIRG 98-1344), and the NIH (R21 RR 12723, D.G.L.) for support, and the NIH (5 T32 HL07327, T.S.B.; 5 T32 GM07281, T.L.S.B.), the American Federation for Aging Research (T.L.S.B.), and the American Foundation for Aging Research (T.L.S.B.) for fellowships.

* To whom correspondence should be addressed at the Department of Pathology, The University of Chicago, 5841 S. Maryland Ave., Chicago, IL 60637-1403. Phone: 773-702-1267. FAX: 773-702-3778. Email: scmeredi@midway.uchicago.edu.

‡ Department of Pathology, The University of Chicago.

§ Current address: Quantum Magnetics, 7740 Kenamar Ct., San Diego, CA 92121.

|| Chemistry Division, Argonne National Laboratory.

⊥ Department of Chemistry, The University of Chicago.

[1] Abbreviations: Aβ, β-amyloid; NMR, nuclear magnetic resonance; APP, β-amyloid precursor protein; A$\beta_{(10-35)}$, peptide comprising residues 10−35 of β-amyloid; DRAWS, dipolar recoupling in a windowless sequence; DQ-DRAWS, double quantum filtered DRAWS; TFA, trifluoroacetic acid; CP/MAS, cross-polarization/magic angle spinning; HMB, hexamethylbenzene; CSA, chemical shift tensor. Standard one- and three-letter abbreviations for amino acids are used throughout the text.

10.1021/bi991527v CCC: $19.00
Published on Web 03/03/2000

peptide (*6, 8*−*12, 14*−*16*). (2) Neurotoxicity is linked with the ability of a peptide to self-associate into β-strand fibrillar aggregates (*45, 62*−*66*). (3) A$\beta_{(10-35)}$ incorporates the core region, point mutations of which impede fibrillogenesis; peptides derived from or based on this region have been used to generate fibrillogenesis inhibitors (*67*−*73*). (4) A$\beta_{(10-35)}$ retains the ability to add to bona fide Alzheimer's plaques, in contrast to other truncated peptides (*74*−*78*). (5) The full-length peptide, A$\beta_{(1-42)}$, is relatively intractable for the controlled formation of fibrils from aqueous media, since at the earliest time points, some of the peptide exists as an amorphous precipitate. In contrast, A$\beta_{(10-35)}$ formed fibrils from aqueous solutions of defined pH, ionic strength, and soluble peptide concentration in a reproducible and controlled fashion, and yielded the homogeneous fibrils needed for structural studies (*17, 76*).

In this paper, NMR experiments, based on the synthetic incorporation of isotopically enriched carbonyl carbons of individual amino acids, have been designed to extend the structural model developed for the core domain across the entire sequence of A$\beta_{(10-35)}$. In all, using a series of ^{13}C-labeled amino acids distributed across the entire sequence, sufficient dipolar constraints will be presented to assign the entire A$\beta_{(10-35)}$ peptide as an in-register, parallel β-sheet within the fibril. Our first goal in the current study was to ascertain whether the structural model developed for the core domain could be extended beyond this limited region, and across the entire sequence of A$\beta_{(10-35)}$. In addition, previous investigations of peptide models of Aβ have shown that fibril diameter and morphology change with both peptide length and sequence (*12, 34*). Such differences might reflect local variations in mobility of the peptide chain, different local conformations within the peptide sequence, conformational heterogeneity among peptide chains within the fibril, or any combinations of these. This situation is common for many amyloidogenic peptides and proteins, and the approaches developed in this study should be generally useful for the investigation of the structure and dynamics of any such self-associating material.

EXPERIMENTAL PROCEDURES

Peptide Synthesis. All peptides reported in these studies were human β-amyloid, amino acids 10 through 35. Peptides were synthesized and purified as reported previously (*17*). Briefly, [1-^{13}C]-L-glycine, [1-^{13}C]-L-leucine, [1-^{13}C]-L-serine, and [1-^{13}C]-L-valine were obtained from Cambridge Isotope Laboratories. Isotopic enrichment of all ^{13}C-labeled amino acids was ≥99%. Protection of the ^{13}C-labeled amino acids was performed by Midwest Biotech, Inc. A$\beta_{(10-35)}$ peptides were synthesized using an FMOC amide resin (PE Biosystems) and, hence, yielded a C-terminal amidated peptide after cleavage. Standard FMOC chemistry was used on an ABI model 431A peptide synthesizer; all nonaliphatic side chains were protected during synthesis, and protecting moieties were removed during cleavage. All histidine and phenylalanine residues were double-coupled. After cleavage from the resin, the peptides were then purified by ether extractions, after which the purity was assessed by analytical HPLC [using a Rainin 25 × 0.5 cm C18 column, a linear gradient over 1 h of 0.1% (v/v) TFA in water to 0.1% TFA in 70/30 acetonitrile/water (v/v), at 70 °C] and the identity confirmed by MALDI-TOF or electron spray mass spectrometry. Peptides determined to be 96−99% pure by this method were stored as the ether precipitate at −20 °C. For some peptides, further purification by preparatory HPLC was required. Preparatory HPLC was performed on a Zorbax 300-SB C4 column at 70 °C under isocratic conditions (27% acetonitrile, 0.1% trifluoroacetic acid).

Fibril Formation. The procedure used to form fibrils has been described in detail elsewhere (*17*). A$\beta_{(10-35)}$ in 100% trifluoroacetic acid (TFA) was precipitated into diethyl ether at 0 °C, and residual TFA was extracted by approximately 10 washes with diethyl ether at 0 °C. Then 50 mg of peptide was dissolved in distilled deionized water to a concentration of ≈0.6 mg/mL (≈0.2 mM); exact concentrations were determined by amino acid analysis. The pH of this solution was 2.9, due to the presence of traces of residual TFA; at this point, no fibrils are precipitable by centrifugation at 17000*g*, nor are fibrils or amorphous precipitate visible by electron microscopy. The pH was then adjusted to 5.60 or 7.40 by the addition of 2 μL aliquots of 0.1 M NaOH every 2 min, with vortexing of the sample between additions of base. The solution was then gently swirled on a rotator plate, at a rate of 0.5 rotation/s, for 36−72 h, under nitrogen. The pH was reverified every 24 h and adjusted when necessary. Aggregation was monitored by HPLC and EM as previously described (*17*). This procedure produces typical amyloid fibrils that are visible by electron microscopy, and stain with Congo red dye, with classic apple green birefringence of the fibrils (*35*); no amorphous precipitate was detectable by electron microscopy. For fibrils formed at pH 7.4, the suspension of fibrils was then flash-frozen using a dry ice/ethanol bath, lyophilized, and stored at −20 °C for solid-state NMR studies. Fibrils formed at pH 7.4 were reexamined by electron microscopy after lyophilization and found to contain fibrils indistinguishable from those evaluated prior to lyophilization.

Aβ fibrils formed at pH 5.6 which are stored at −20 °C have been shown to denature (*36*). Similarly, we found that lyophilization disrupted fibrils formed at pH 5.6, but not those formed at pH 7.4. To examine this phenomenon further, a series of NMR experiments on nonlyophilized peptides was initiated. For studies of nonlyophilized peptide, fibrils formed at pH 5.6 were harvested by centricon filtration, and the samples were then flash-frozen. The NMR studies were performed by immediately transferring these samples directly into an NMR instrument rotor cooled with liquid nitrogen, which maintains the spectrometer probe at −80 °C, and the DRAWS experiment was performed. After 2 weeks of storage in a −20 °C freezer, the same pH 5.6 and 7.4 samples were again studied by DRAWS, at which time no contact was observed in the pH 5.6 sample; the samples were also examined by electron microscopy.

Solid-State NMR Experiments. Solid-state NMR methods used for this work have been described in detail elsewhere (*17, 18, 37, 38*). Briefly, cross-polarization/magic angle spinning (CP/MAS) ^{13}C NMR experiments were performed on a Bruker Advance DSX spectrometer tuned to a frequency of 50.3 MHz. The DRAWS and DQ-DRAWS pulse sequences were implemented (*17, 18, 37, 38*). Lyophilized peptide samples were mixed with 8−12 mg of HMB and packed into 5 mm Bruker rotors containing 4 mm spacers at each end. If the peptide/HMB samples did not entirely fill the rotor, the samples were unpacked and mixed with a small

amount of KBr to take up the space. Unless otherwise noted, experiments were performed at room temperature. In some cases, as noted in the text, fibril preparations were flash-frozen in NMR rotors using liquid nitrogen and inserted into the precooled spectrometer for experiments at −80 °C. In all cases, samples were spun at 4525 (±3) Hz. The ^{13}C RF power level was set to 38.5 kHz. The ^{1}H decoupling level was 120 kHz. To allow the samples and electronics to reach equilibrium, samples were pulsed for 2 h prior to acquisition of DRAWS data points, during which time ^{1}H and ^{13}C power and tuning were checked and double-checked. DRAWS spectra were acquired with 272−476 transients. Data points for a single DRAWS curve typically required 1−4 h of data acquisition; data points in the plots shown below were the average values from five independent NMR experiments; at least three replicate samples of each peptide were examined in this way. Spectra from DRAWS experiments were processed and analyzed as previously described (*17, 18, 37*). In addition, because in solid-state NMR virtually all β-sheet carbonyl chemical shifts are superimposable at 171 ppm (*39*), it was necessary to subtract the natural-abundance signal derived from other amino acid residues; this was done as described previously (*17, 18*).

Numerical Simulations. Simulated data were created by numerical calculation using a density matrix approach (*18, 37*). Briefly, the input parameters to the numerical calculation program included the chemical shift tensor (CSA) elements for the spin-1/2 nuclei, the dipolar coupling strengths, Euler angles which rotate the CSA tensors from the molecular frame to their respective principal axis systems, an initial density matrix $\rho(0)$, an observable, and any relevant relaxation parameters. In this work, the Euler angles were set to zero, as it was determined that they had a negligible effect on the simulated curves. The CSA parameters were taken from Ye et al. (*39*). The dipolar coupling strength (d) was calculated from the equation:

$$d = 7.598 \times 10^{-27}/r^3$$

where r is the distance of separation (in meters) between two nuclei.

Relaxation effects were modeled by multiplying the single quantum density matrix elements by an exponential factor at the end of each time increment. Data from the unlabeled sample were used to determine the appropriate single quantum relaxation constant in the absence of an enriched nucleus. A powder average of 2000 randomly selected crystallite orientations was performed.

As we report in detail elsewhere (*18*), spin simulations were performed using a three-spin, infinite-loop model for fibril samples. In analyzing DRAWS data, our procedure was to model relaxation data according to numerical distance simulations. These simulations, however, must take into account the effects of the number of interacting spins and the various multiple spin geometries, both of which are considered in detail in another paper (*18*). Briefly stated, initial DRAWS results with peptides singly labeled with ^{13}C in carbonyl carbon atoms of residues 15−18 of the "core region" were calculated using "two-spin" and "three-spin" models, and the three-spin model with a distance of 5.0 ± 0.2 Å provided a much better fit to the experimental data. Spin simulations were first performed using a model in which three spins are located at the vertexes of an equilateral triangle. While this geometry was the simplest to calculate, it was unrealistic as a model of amyloid parallel β-sheets; performing density matrix calculations on such a large number of spins turns out to be impractical, however. For this reason, we chose to study the influence of different geometries on the simulations involving three spins, each located at the vertexes of an equilateral triangle, and four spins, with each spin located at the vertexes of a square. The results for the two geometries were almost identical at the initial decay rates, i.e., prior to the onset of the dipolar oscillations seen at the shorter distances. In the case of simulations for a 5 Å distance, both models gave the same result for DRAWS mixing times approaching 20 ms, indicating that all 5 Å simulation models in which every spin interacts with two others of equal magnitude will be indistinguishable. In addition, to test geometries that are more representative of fibril structure, we simulated multiple-spin systems in a linear arrangement and compared the results with those obtained for the triangular model. The 5 Å simulation curves for linear versus triangular geometries are fairly similar and appear to become convergent as the number of spins applied to the linear model increases.

We have shown elsewhere (*18*) that for fibrillar samples of Aβ, T_2^{SQ} relaxation times of carbonyl carbons measured in the presence of DRAWS irradiation are very similar for all samples investigated, $T_2^{SQ} \approx 19$ ms; similar values have been obtained previously for carbonyl (unprotonated) carbons in other systems (*80*). Furthermore, DRAWS T_2^{SQ} values were similar regardless of the magnitude of T_2^{SQ} relaxation times measured in the Hahn spin−echo experiment. Hence, our previous analysis used the reasonable assumption that T_2^{SQ} values would also follow a similar trend in the presence of DRAWS r.f. irradiation. Moreover, T_2^{SQ} values measured for all amyloid samples tend to be similar. On the basis of these arguments and the previously observed behavior of R_2^{SQ} on the outcome of the DRAWS simulations on doubly labeled samples (see reference *18*), the effects of DQ relaxation could be neglected in our analyses of fibrillar Aβ samples. For the simulations of the nonfibrillar TFA/ether preparations, a double quantum dephasing rate of $T_2^{DQ} = 14$ ms was calculated to give the best fit of the data; there was no dispersion of distances. In addition, a 0.25 Å dispersion of distances was used; i.e., several distances from 2.8 to 4.1 Å were simulated in 0.05 Å intervals. These calculated curves were added together using a normal distribution centered at 3.4 Å with a width of 0.25 Å as a weighting function.

RESULTS

Confirmation of Fibril Morphology and Stability. Electron microscopy was initially used to evaluate environmental conditions necessary to prepare stable and homogeneous fibrils. As shown in Figure 1, fibrils were formed at pH 5.6 and 7.4, and a significant number existed as superhelical pairs. The repeat distance of this twist was ≈600 Å, and the diameters were ≈90 Å by ≈160 Å. At pH 7.4, in addition to the twisted pairs, more highly aggregated bundles of single fibrils having a diameter of ≈80 Å are obtained. Both conditions proved suitable for preparing homogeneous fibrils for solid-state NMR experiments.

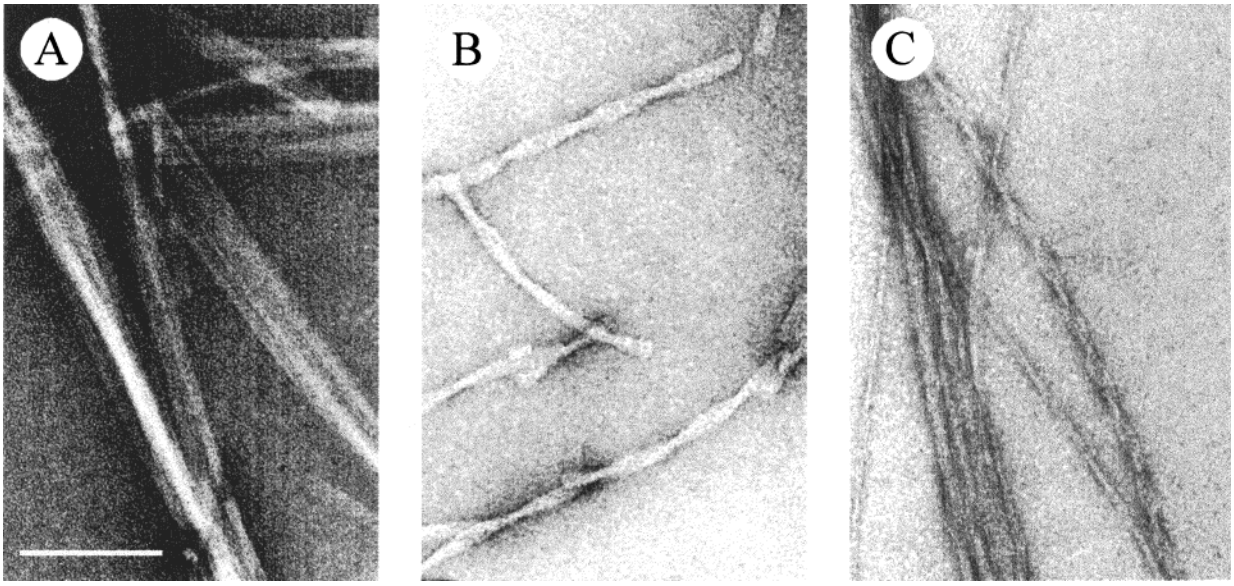

FIGURE 1: Electron microscopy of A$\beta_{(10-35)}$ fibrils prepared at (A) pH 3, (B) pH 5.6, and (C) pH 7.4. Samples were applied to a glow-discharge 400 mesh carbon-coated support film, followed by staining with 1% uranyl acetate. Micrographs were recorded using Philips EM 300 at magnifications of 33750×. The scale bar represents 100 nm.

Fibrils formed at pH 7.4 were stable to lyophilization Furthermore, electron microscopy showed the classical amyloid fibrils but no amorphous precipitates. In contrast, after lyophilization the samples prepared at pH 5.6 contained a mixture of amorphous precipitates and fibrils when examined by electron microscopy. As discussed under Experimental Procedures, fibrils formed at pH 5.6 were prone to loss of the contact in DRAWS experiments. In all cases, the loss of the contact in DRAWS experiments was associated with the absence of fibrils when the samples were subsequently examined by electron microscopy. These findings are in accord with those of Wood et al. (*79*). For these reasons, most of the experiments reported below involved fibril samples prepared at pH 7.4.

i to i + 1 Labeled Carbonyls as Probe for Secondary Structure. Shown below is the amino acid sequence of A$\beta_{(10-35)}$:

^{10}YEVHHQKLVFFAEDVGSNKGAIIGL^{35}M

In previous work, the core residues ^{15}QKLV of A$\beta_{(10-35)}$ were shown to exist in the Aβ fibril as a parallel β-sheet (*17*). Figure 2 shows representative 1D ^{13}C-MAS spectra of fibrils prepared from [1-^{13}C]-Val$_{18}$-A$\beta_{(10-35)}$ at pH 7.4, and a nonfibrillar sample precipitated directly from 100% TFA into diethyl ether (pH ≈ 3.0). At pH 7.4 (Figure 2B), the carbonyl resonance appeared at 170.9 ppm. This shift was consistent with that expected for valine restrained in a β-conformation, δ 171.5 (*40*). When the peptide was precipitated from 100% TFA with diethyl ether (pH ≈ 3.0, Figure 2A), a resonance was observed at 175.2 ppm. This chemical shift is consistent with valine existing in an α-helix conformation, 174.9 ppm (*40*).

Carbonyl−carbonyl distances were measured directly using dipolar recoupling NMR methods. Molecular modeling performed on the basis of X-ray diffraction data on peptide structures available in the Brookhaven Protein Data Bank predicts that carbonyls in adjacent residues in canonical α-helices have separations in the range of 2.9−3.1 Å (Figure 3A). Extended as β-strands, this distance increases to 3.3−3.5 Å. The ether-precipitated and fibrillized samples gave significantly different dephasing rates (Figure 3B). When simulated using a relaxation parameter of $R_2 = 58$ s^{-1}, distances of 3.0 ± 0.1 and 3.5 ± 0.1 Å, respectively, were determined. The fibrilized preparation therefore demonstrated a β-strand secondary structure, consistent with the determined chemical shifts of the carbonyls and the previous interstrand measurements within this region of A$\beta_{(10-35)}$ (*17, 18*). In the context of the ether precipitate, Aβ has been found to adopt α-helical conformations in membrane-mimicking solvents (*41*), and, indeed, an α-helical conformation is believed to

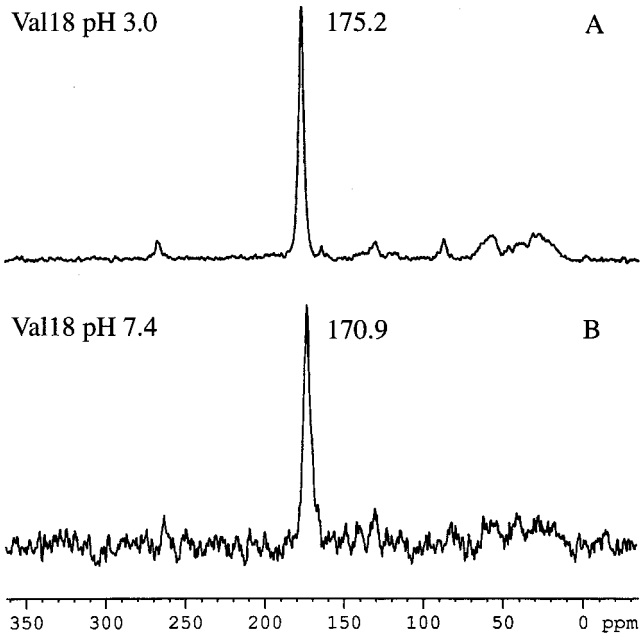

FIGURE 2: Representative 1D ^{13}C-MAS spectra of samples prepared from [1-^{13}C]-Val$_{18}$-A$\beta_{(10-35)}$. Figure 2A shows a nonfibrillar sample precipitated directly from 100% TFA into diethyl ether (pH ≈ 3.0). Figure 2B shows a fibrillar sample of the same peptide prepared at pH 7.4. Figure 2A is the result of 256 scans on a sample containing 50 mg of peptide; Figure 2B is the result of 16 scans on 50 mg of peptide.

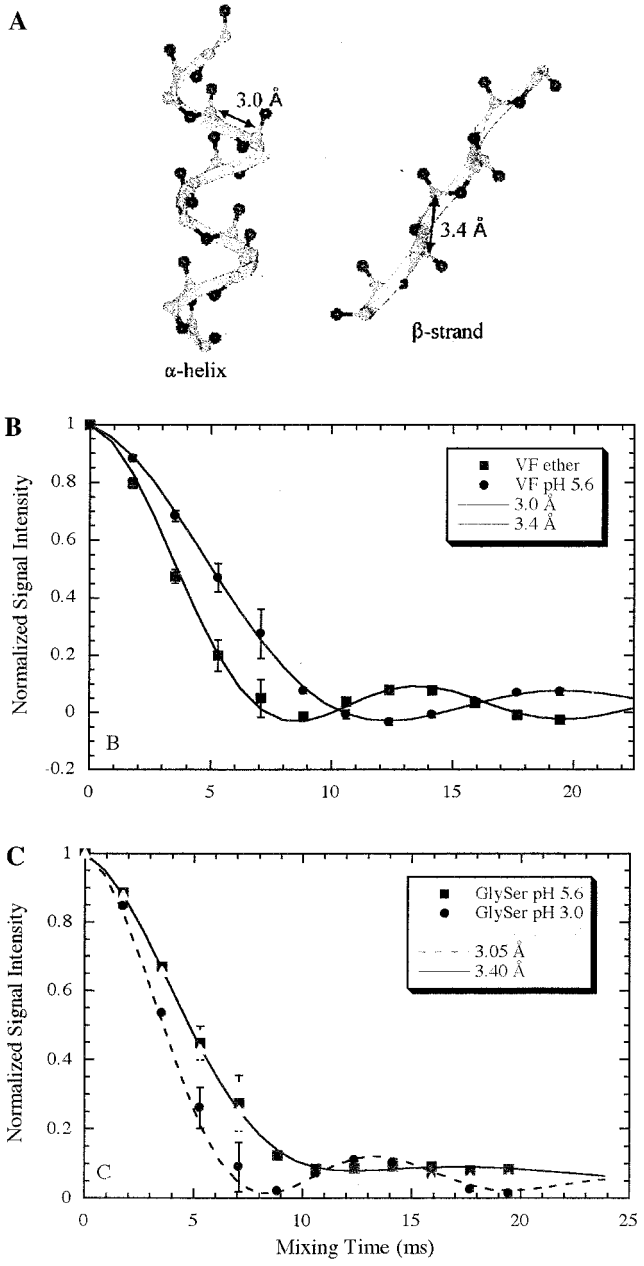

FIGURE 3: (A) Predicted *i*, *i* + 1 carbonyl−carbonyl distances for α-helical (3.0 Å) and *β*-strand (3.4 Å) conformations. (B) [1-^{13}C]-Val$_{18}$-[1-^{13}C]-Phe$_{19}$-A$\beta_{(10-35)}$ was prepared either as a diethyl ether precipitate from TFA or as fibrils formed at pH 5.6. Data shown are for 50 mg samples ± SD (n = 5) and analyzed by DRAWS. Two-spin simulations were calculated under the DRAWS Hamiltonian, and the curves obtained for 3.0 and 3.4 Å distances are shown. (C) DRAWS experiment on [1-^{13}C]-Gly$_{25}$-[1-^{13}C]-Ser$_{26}$-A$\beta_{(10-35)}$ obtained under the same conditions.

be the native conformation this region of the *β*-amyloid precursor protein (APP) from which A*β* is generated in vivo (*4*, *34*, *42*). This evidence is consistent with the proposal that under fibril-dissolving conditions, in this case strong acid, the peptide adopts an α-helical conformation.

Extension of the Parallel β-Strand, Determined by Further ^{13}C Labeling and Solid-State NMR. In our previous experiments, 1-^{13}C-labels at positions 15−18 (boldface, underlined)

^{10}YEVHH**QKLV**FFAEDVGSNKGAIIGL^{35}M

were used to determine a parallel, directly aligned structure for this core domain of A$\beta_{(10-35)}$ (*17*). Additional peptides were synthesized to examine whether this structure is propagated beyond the core domain. The predicted distance between carbonyls of like residues along a parallel *β*-sheet in-register would be ≈5 Å, a distance well within the range of measurement by the DRAWS technique. To determine whether the parallel, aligned *β*-structure is propagated, additional peptides were synthesized, each containing a single amino acid labeled with ^{13}C at the carbonyl carbon. The results of these experiments will be presented in two sections: (1) the residues around a potential turn sequence; (2) additional hydrophobic residues, including ones at each terminus of the peptide.

Investigation of the Putative Turn at Residues 25−30.

^{10}YEVHHQKLVFFAEDV**GS**NK**G**AII**G**L^{35}M

A turn sequence, predicted by the algorithm of Chou and Fasman (*43*) across residues 25−30, has been proposed for A*β* (*7*, *14*−*16*, *44*) and investigated by Pike (*45*). A peptide containing two labeled residues at the start of the potential turn domain, [1-^{13}C]-Gly$_{25}$-[1-^{13}C]-Ser$_{26}$-A$\beta_{(10-35)}$, was synthesized. Samples were prepared at pH ≈ 3.0; despite incubation times which were up to a week longer than those needed to form fibrils at pH 5.6 or 7.4, at pH 3.0 fibril formation was slowed or prevented completely, as shown by the persistence of monomer in HPLC analyses, and the absence of fibrils by EM (Figure 1A). The measured carbonyl−carbonyl distance was 3.0 Å (Figure 3C), most consistent with an α-helical conformation. At both pH 5.6 and pH 7.4, however, the relaxation data were best simulated with the longer distance of ≈3.4 Å. While this distance is consistent with a *β*-conformation, at longer mixing times the expected oscillations in the DRAWS curve were significantly dampened, and curve-fitting analyses were modified to account for greater heterogeneity in the sample.

The single-labeled [1-^{13}C]-Gly$_{25}$- and [1-^{13}C]-Ser$_{26}$-A$\beta_{(10-35)}$ were prepared to evaluate the interstrand distances. As shown in Figure 4, contact distances in fibrils prepared at pH 7.4 were significantly longer than those observed over the core segment of the peptide with Gly$_{25}$ = 5.7 ± 0.2 Å and Ser$_{26}$ = 5.6 ± 0.2 Å. Taken together with the parallel *β*-conformation established for the core region of the peptide, both the inter- and intrastrand distances established with Gly$_{25}$ and Ser$_{26}$ are only consistent with a parallel *β*-structure extending through this region as well. Glycine residues are the most conformationally flexible of the natural amino acids, and peptides containing [1-^{13}C]-Gly$_{29}$ and [1-^{13}C]-Gly$_{33}$ were prepared to determine if this anticipated flexibility might contribute to the measured interstrand differences. Indeed, both measured distances with the Gly$_{29}$ and Gly$_{33}$ carbonyl-labeled peptides were larger, 5.5 ± 0.2 and 5.8 ± 0.2 Å, respectively (Figure 4).

Evaluation of the N- and the C-Terminus: Evaluation of Additional Internal Hydrophobic Residues.

^{10}YE**V**HHQKLVF**F**AED**V**GSNKGAIIG**L**^{35}M

Both [1-^{13}C]-Val$_{12}$- and [1-^{13}C]-Leu$_{34}$-A$\beta_{(10-35)}$ were prepared to evaluate dipolar contacts at the extreme N- and C-terminal ends, respectively. The interstrand distance between the Leu$_{34}$ carbonyls was found to be 4.9 ± 0.2 Å (Figure 5). Such a close contact was surprising given that

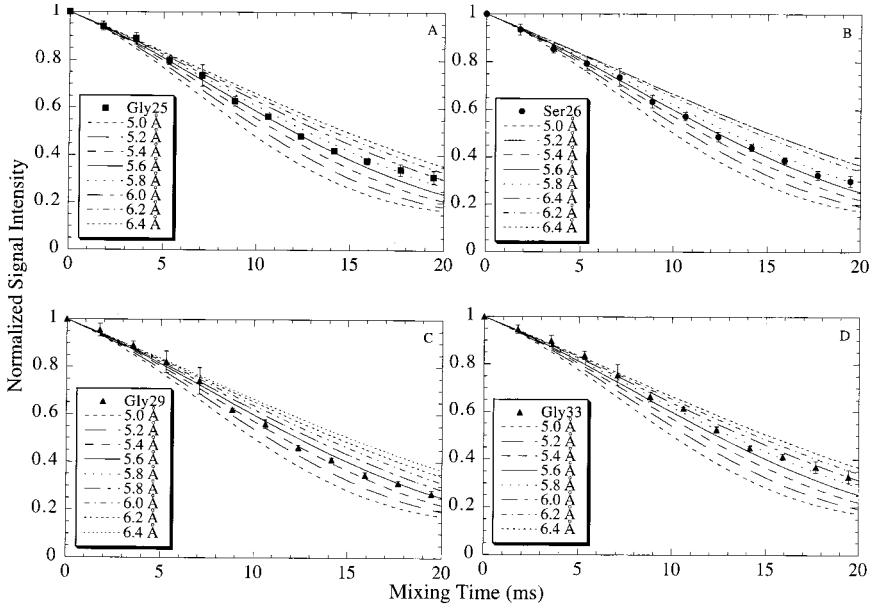

FIGURE 4: Examination of interpeptide distances at Gly_{25}, Ser_{26}, Gly_{29}, and Gly_{33}. Peptides containing 1-^{13}C-labeled amino acids at positions 25, 36, 29, and 33 in the A$\beta_{(10-35)}$ sequence were synthesized, fibrillized at pH 7.4, lyophilized, and examined under the DRAWS conditions as described. All data shown represent the mean of 5 experiments (±SD) obtained for 50 mg samples (≈256 scans). The data for Gly_{25} (squares, A), Ser_{26} (circles, B), Gly_{29} (triangles, C), and Gly_{33} (triangles, D) fit best for distances at 5.7 (±0.2), 5.6 (±0.2), 5.5 (±0.2), and 5.7 (±0.2) Å, respectively. Error bars are displayed only when they exceed the symbol size.

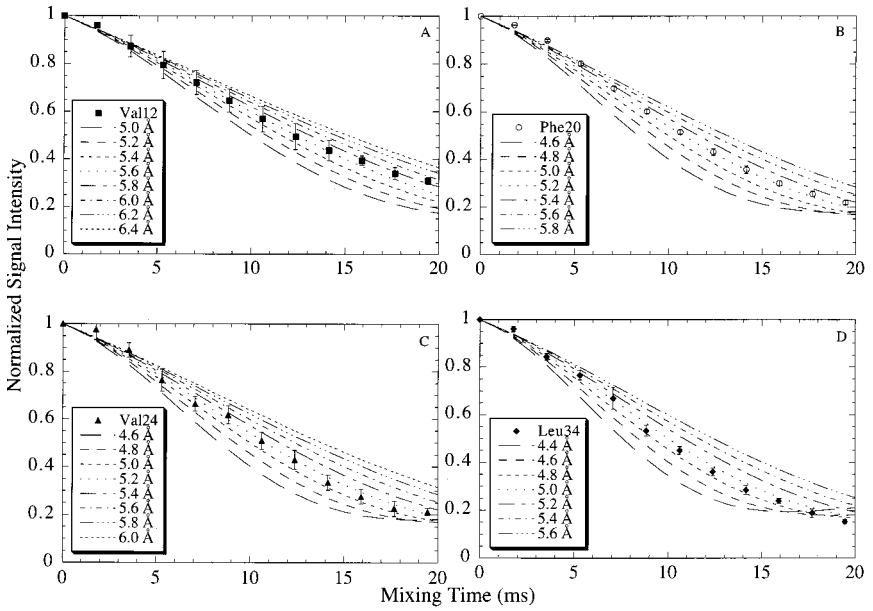

FIGURE 5: Examination of interpeptide distances at Val_{12}, Phe_{20}, Val_{24}, and Leu_{34}. Peptides containing 1-^{13}C-labeled amino acids at positions 12, 20, 24, and 34 in the A$\beta_{(10-35)}$ sequence were synthesized, prepared at pH 7.4, lyophilized, and examined under the DRAWS conditions. For Phe_{20}, Val_{24}, and Leu_{34}, data represent the mean of 5 experiments (±SD) obtained for 50 mg samples (≈256 scans). Phe_{20} (circles, B), Val_{24} (triangles, C), and Leu_{34} (diamonds, D) give measured distances of 5.2 (±0.2), 5.1 (±0.2), and 4.9 (±0.2) Å, respectively. For Val_{12}, the data represent the mean of two 50 mg sample preparations (±SD, $n = 10$), and the interstrand distance is 5.7 (±0.3) Å. Error bars are displayed only when they exceed the symbol size.

Leu_{34} is positioned on the C-terminal side of Gly_{33}, a residue shown above to have an interstrand distance of 5.8 Å. At the N-terminus, fibrils prepared from [1-^{13}C]-Val_{12}-A$\beta_{(10-35)}$ gave a 5.7 ± 0.3 Å interstrand distance (Figure 5). Such longer distances are unlikely to be a function of β-branching in the side chains as fibrils prepared from [1-^{13}C]-Val_{18}-A$\beta_{(10-35)}$ gave a distance of 5.1 Å, and [1-^{13}C]-Val_{24}-A$\beta_{(10-35)}$, located on the N-terminal side of Gly_{25}, also showed a 5.1 ± 0.2 Å distance. [1-^{13}C]-Phe_{20}-A$\beta_{(10-35)}$, located at the C-terminal side of the central hydrophobic region, also gave a 5.2 ± 0.2 Å distance. Therefore, while there is some variation along the sequence, these measurements made across the length of A$\beta_{(10-35)}$ were consistent only with each residue in the fibril existing as an in-register parallel β-sheet equally positioned between two like strands of the same orientation and conformation.

DISCUSSION

In this paper we demonstrate that the parallel β-sheet structure, with like residues in-register, is observed not only for the central core region of A$\beta_{(10-35)}$ but also through the entire length of the peptide. Specific cross-linking reactions

carried out on the forming fibrils of A$\beta_{(10-35)}$ identified areas of close contact between adjacent peptide molecules, and thus allowed for the synthetic incorporation of specific isotopic labels for the measurement of interatomic distances within the core region (*17*). On the C-terminal side of the core region, at Phe_{20}, Val_{24}, and Leu_{34}, interpeptide distances of 5.2, 5.1, and 4.9 ($\pm$0.2) Å, respectively, were observed, distances compatible only with the extension of the parallel β-strand across the entire length of this peptide. The slightly longer distance of 5.7 Å between Val_{12} residues close to the N-terminus suggests continuation of the parallel β-structure to the amino terminus, though perhaps with some fraying, a common finding near the termini of peptides. In addition, a turn structure is predicted within the Aβ sequence by the Chou−Fasman algorithm as well as physical data on other related peptides (*7, 14−16, 43−45*). Lee et al. (*44*) observed a possible turn signature by NMR in dilute solutions of A$\beta_{(10-35)}$, though at a slightly different locus, amino acids 21−25. The distances observed in the studies reported above for Val_{24}, Gly_{25}, Ser_{26}, and Gly_{29} are all incompatible with any known canonical turn, and indeed are consistent with only a parallel β-sheet in-register. By measuring interstrand distances down the length of the peptide, skipping no more than three residues, sufficient information was obtained to establish that the entire A$\beta_{(10-35)}$ peptide exists as an in-register parallel β-sheet within the fibril.

Because of the $1/r^3$ dependence of the dipolar coupling, the closest contact between two labeled sites dominates the distance measurement. Therefore, intrastrand measurements can be made with precision even in the presence of weaker interstrand interactions. However, a particularly powerful feature of these experiments has been the ability to distinguish between single and multiple long-distance interactions (*17, 18*). Molecular modeling within existing β-structures places bounds for the carbonyl to carbonyl distances of between 4.8 and 5.0 Å, depending on the pleat of the sheet (*17*). Since the measured distances are derived from an average distance across all the peptides in the sheet, peptides that have no dipolar contact will relax slower and contribute to an overall lengthening of the experimentally measured distance. The accuracy of these measurements, and their correspondence to the carbonyl−carbonyl distances predicted for parallel β-sheets, argues convincingly for the homogeneity of the propagating array in the A$\beta_{(10-35)}$ fibril.

The interstrand distances for Val_{12}, Gly_{25}, Ser_{26}, and Gly_{29}, however, are longer than those observed across the other residues. Explanations for these longer distance determinations, and the apparent dampened oscillations in the Gly_{25}−Ser_{26} double-labeled samples, have several possible origins including averaging effects resulting from greater disorder in this region of the peptide, and overdamping as a result of DQ relaxation processes and/or additional weak internuclear interactions. We have argued that T_2^{DQ} can be generally neglected in these studies and that the relaxation processes are more akin to $T_{1\rho}$ than T_2 under the DRAWS conditions (*18*). The observation that data for the Gly_{25}−Ser_{26} double-labeled peptide were best modeled by incorporating a parameter of $T_2^{DQ} = 10$ ms and a 0.25 Å dispersion of distances into the calculations, together with the slightly longer interstrand distances measured for the single-labeled residues in this region, argues that there is either a greater mobility and/or a greater static heterogeneity associated with these residues in the fiber. In that regard, the distances measured for all three glycine residues in A$\beta_{(10-35)}$ give a longer carbonyl−carbonyl distance consistent with the greater flexibility associated with this residue. However, the greater distances are not unique to glycine, as Val_{12} shows a 5.7 Å interstrand dipolar contact, and this heterogeneity is probably a characteristic of specific regions of the peptide. This flexibility/disorder does appear to be very localized in the fibril as Leu_{34}, one residue from the C-terminus and just on the C-terminal side of Gly_{33}, appears both motionally restricted and positionally fixed with an interstrand distance of 4.9 Å. A further analysis of how side chain structure might contribute to this flexibility and/or fibril heterogeneity will be important for a complete understanding of fibril dynamics and morphology.

There are several consequences of this extended array of in-register, parallel, β-strands in the A$\beta_{(10-35)}$ fibrils. This structure results in the amplification of the inherent amphiphilic character of the peptide across the entire repeated

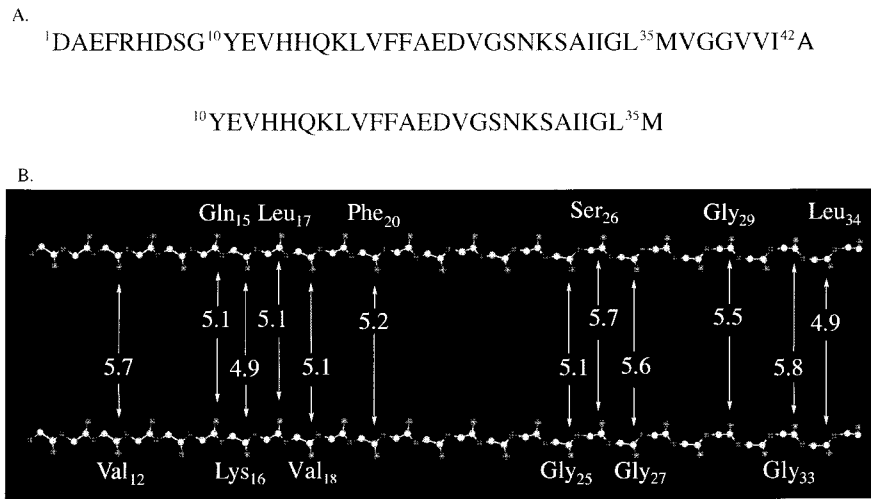

FIGURE 6: Structural unit for A$\beta_{(10-35)}$ determined by NMR experiments. (A) Amino acid sequence of full-length Aβ and A$\beta_{(10-35)}$. (B) β-Strand model of the peptide backbone of two adjacent A$\beta_{(10-35)}$ molecules in the long axis of a fibril. Each of the carbonyl carbons examined by solid-state NMR is indicated, with inter-carbonyl distances given in angstroms (Å). At each of these positions, an interstrand contact distance of $\approx$5 Å was found using the DRAWS technique, for samples prepared at pH 7.4.

stack of the β-sheet. The understanding of the consequences of this arrangement was exploited in the construction of the PEG block copolymer as a strategy to generate Aβ fibrils whose formation was completely reversible (*46*). In addition, the repeated stacking of identical aliphatic side chains, such as Ala, Val, and Leu, and the aromatic Phe side chains is a common feature known to stabilize the extended β-sheets found in crystal structures of β-helices (*47*−*49*). This arrangement also places the planar histidine residues in alignment (Figure 6). Several studies suggest that Zn^{2+} ions may increase the rate of Aβ fibrillogenesis, though such ions are not necessary for fibrillogenesis (*36*, *50*−*58*). The in-register parallel β-sheet structure would place His_{13} and His_{14} of adjacent β-strands in close proximity, possibly allowing them to bind Zn^{2+} or other divalent metal ions. Such metal binding might, in turn, stabilize the in-register parallel β-strand conformation, and facilitate the formation of Aβ fibrils.

To facilitate the preparation of homogeneous fibrils, the truncated peptide model, $A\beta_{(10-35)}$, was used as a model for the full-length $A\beta_{(1-40)}$ and $A\beta_{(1-42)}$ in these studies. An antiparallel structure has been proposed for residues 34−42 on the basis of solid-state NMR studies of a doubly ^{13}C-labeled nonapeptide (*59*), and this proposal has been incorporated into a recent structural model of Aβ (*60*). Energetic models of amyloids have supported both parallel and antiparallel β-strand organizations (*61*), and other models have incorporated an ensemble of conformational species within amyloid fibrils (*5*). These studies suggest that the full-length peptide could exist as a parallel β-sheet and have established methods sufficient for its full characterization. It is possible that the full-length peptide exists in a parallel arrangement but diverges from this pattern near the termini; or that it does not diverge from this pattern; or, alternatively, that it differs radically from the truncated peptide. In any of these cases, the approach taken in these studies should now allow for the full characterization of the structure of the full-length peptide. Such studies will continue to expand our understanding of the structure and dynamics of the fibril arrays formed by the amyloidogenic peptides and proteins.

ACKNOWLEDGMENT

Electron microscopy was performed by Robert Josephs at The University of Chicago.

REFERENCES

1. Glenner, G. G., and Wong, C. W. (1984) *Biochem. Biophys. Res. Commun. 122*, 1131−1135.
2. Masters, C. L., Simms, G., Weinman, N. A., Multhaup, G., McDonald, B. L., and Beyreuther, K. (1985) *Proc. Natl. Acad. Sci. U.S.A. 82*, 4245−4249.
3. Prelli, F., Castano, E., Glenner, G. G., and Frangione, B. (1988) *J. Neurochem. 51*, 648−651.
4. Kang, J., Lemaire, H. G., Unterbeck, A., Salbaum, J. M., Masters, C. L., Grzeschik, K. H., Multhaup, G., Beyreuthe, K., and Muller-Hill, B. (1987) *Nature 325*, 733−736.
5. Teplow, D. B. (1998) *Amyloid: Int. J. Exp. Clin. Invest. 5*, 121−142.
6. Castano, E. M., Ghiso, J., Prelli, F., Gorevic, P. D., Migheli, A., and Frangione, B. (1986) *Biochem. Biophys. Res. Commun. 141*, 782−789.
7. Kirschner, D. A., Inouye, H., Duffy, L. K., Sinclair, A., Lind, M., and Selkoe, D. J. (1987) *Proc. Natl. Acad. Sci. U.S.A. 84*, 6953−6957.
8. Gorevic, P. D., Castano, E. M., Sarma, R., and Frangione, B. (1987) *Biochem. Biophys. Res. Commun. 147*, 854−862.
9. Halverson, K., Fraser, P. E., Kirschner, D. A., and Lansbury, P. T., Jr. (1990) *Biochemistry 29*, 2639−2644.
10. Fraser, P. E., Duffy, L. K., O'Malley, M. B., Nguyen, J., Inouye, H., and Kirschner, D. A. (1991) *J. Neurosci. Res. 28*, 474−485.
11. Fraser, P. E., Nguyen, J. T., Surewicz, W. K., and Kirschner, D. A. (1991) *Biophys. J. 60*, 1190−1201.
12. Fraser, P. E., Nguyen, J. T., Inouye, H., Surewicz, W. K., Selkoe, D. J., Podlisny, M. B., and Kirschner, D. A. (1992) *Biochemistry 31*, 10716−10723.
13. Hilbich, C., Kisters-Woike, B., Reed, J., Masters, C. L., and Beyreuther, K. (1991) *J. Mol. Biol. 218*, 149−163.
14. Barrow, C. J., and Zagorski, M. G. (1991) *Science 253*, 179−182.
15. Barrow, C. J., Yasuda, A., Kenny, P. T., and Zagorski, M. G. (1992) *J. Mol. Biol. 225*, 1075−1093.
16. Burdick, D., Soreghan, B., Kwon, M., Kosmoski, J., Knauer, M., Henschen, A., Yates, J., Cotman, C., and Glabe, C. (1992) *J. Biol. Chem. 267*, 546−554.
17. Benzinger, T. L. S., Gregory, D. M., Burkoth, T. S., Miller-Auer, H., Lynn, D. G., Botto, R. E., and Meredith, S. C. (1998) *Proc. Natl. Acad. Sci. U.S.A. 10*, 13407−13412.
18. Gregory, D. M., Benzinger, T. L. S., Burkoth, T. S., Miller-Auer, H., Lynn, D. G., Meredith, S. C., and Botto, R. E. (1998) *Solid State Nucl. Magn. Reson. 13*, 149−166.
19. Eaton, W. A., and Hofrichter, J. (1990) *Adv. Protein Chem. 40*, 63−279.
20. Zinkernagel, R. M. (1997) *Biol. Chem. 378*, 725−729.
21. Schroder, J. M. (1993) *Brain Pathol. 3*, 177−190.
22. Ohtsuki, I., and Nagano, K. (1982) *Adv. Biophys. 15*, 93−130.
23. Horne, R. W. (1978) *J. Microsc. 113*, 241−256.
24. Heine, H., and Schaeg, G. (1977) *Virchows Arch. A: Pathol. Anat. Histol. 376*, 89−94.
25. Knight, D. P., and Hunt, S. (1976) *Tissue Cell 8*, 183−193.
26. Magdoff-Fairchild, B., and Chiu, C. C. (1979) *Proc. Natl. Acad. Sci. U.S.A. 76*, 223−226.
27. Ellis, M. J., Knapp, S., Koeck, P. J., Fakoor-Biniaz, Z., Ladenstein, R., and Hebert, H. (1998) *J. Struct. Biol. 123*, 30−36.
28. Molnar, M., and Schroder, J. M. (1998) *Acta Neuropathol. 96*, 41−51.
29. Geisler, N., Schunemann, J., Weber, K., Haner, M., and Aebi,U. (1998) *J. Mol. Biol. 282*, 601−617.
30. Bouchard, M., Pare, C., Dutasta, J. P., Chauvet, J. P., Gicquaud, C., and Auger, M. (1998) *Biochemistry 37*, 3149−3155.
31. Taylor, K. A., Tang, J., Cheng, Y., and Winkler, H. (1997) *J. Struct. Biol. 120*, 372−386.
32. Kupcu, S., Sleytr, U. B., and Sara, M. (1996) *J. Immunol. Methods 196*, 73−84.
33. Zhang, R., Tristram-Nagle, S., Sun, W., Headrick, R. L., Irving, T. C., Suter, R. M., and Nagle, J. F. (1996) *Biophys. J. 70*, 349−357.
34. Dyrks, T., Dyrks, E., Masters, C. L., and Beyreuther, K. (1993) *FEBS Lett. 324*, 231−236.
35. Jurnak, F., Yoder, M. D., Pickersgill, R., and Jenkins, J. (1994) *Curr. Opin. Struct. Biol. 4*, 802−806.
36. Huang, X., Atwood, C. S., Moir, R. D., Hartshorn, M. A., Vonsattel, J.-P., Tanzi, R. E., and Bush, A. I. (1997) *J. Biol. Chem. 272*, 26464−26470.
37. Gregory, D. M., Mehta, M. A., Shiels, J. C., and Drobny, G. P. (1997) *J. Chem. Phys. 107*, 28−42.
38. Gregory, D. M., Wolfe, G. M., Jarvie, T. P., Sheils, J. C., and Drobny, G. P. (1996) *Mol. Phys. 89*, 1835−1849.
39. Ye, C., Fu, R., Hu, J., Hou, L., and Ding, S. (1993) *Magn. Res. Chem. 31*, 699.
40. Saitô, H. (1986) *Magn. Res. Chem. 24*, 835−852.
41. Zagorski, M. G., and Barrow, C. J. (1992) *Biochemistry 31*, 5621−5631.
42. Selkoe, D. J., Podlisny, M. B., Joachim, C. L., Vickers, E. A., Lee, G., Fritz, L. C., and Oltersdorf, T. (1988) *Proc. Natl. Acad. Sci. U.S.A. 85*, 7341−7345.

43. Chou, P. Y., and Fasman, G. D. (1978) *Annu. Rev. Biochem. 47*, 251−276.
44. Lee, J. P., Stimson, E. R., Ghilardi, J. R., Mantyh, P. W., Lu, Y. A., Felix, A. M., Llanos, W., Behbin, A., Cummings, M., Van Criekinge, M., Timms, W., and Maggio, J. E. (1995) *Biochemistry 34*, 5191−5200.
45. Pike, C. J., Walencewicz-Wasserman, A. J., Kosmoski, J., Cribbs, D. H., Glabe, C. G., and Cotman, C. W. (1995) *J. Neurochem. 64*, 253−265.
46. Burkoth, T. S., Benzinger, T. L. S., Jones, D. N. M., Hallenga, K., Meredith, S. C., and Lynn, D. G. (1998) *J. Am. Chem. Soc. 120*, 7655−7656.
47. Cohen, F. E. (1993) *Science 260*, 1444−1445.
48. Jurnak, F., Yoder, M. D., Pickersgill, R., and Jenkins, J. (1994) *Curr. Opin. Struct. Biol. 4*, 802−806.
49. Nesloney, C. L., and Kelly, J. W. (1996) *Bioorg. Med. Chem. 4*, 739−766.
50. Bush, A. I., Pettingell, W. H., Jr., Paradis, M. D., and Tanzi, R. E. (1994) *J. Biol. Chem. 269*, 12152−12158.
51. Bush, A. I., Pettingell, W. H., Multhaup, G., de Paradis, M., Vonsattel, J. P., Gusella, J. F., Beyreuther, K., Masters, C. L., and Tanzi, R. E. (1994) *Science 265*, 1464−1467.
52. Bush, A. I., Moir, R. D., Rosenkrancz, K. M., and Tanzi, R. E. (1995) *Science 268*, 1921−1922.
53. Garzon-Rodriguez, W., Sepulveda-Becerra, M., Milton, S., and Glabe, C. G. (1997) *J. Biol. Chem. 272*, 21037−21044.
54. Assaf, S. Y., and Chung, S. H. (1984) *Nature 308*, 734−736.
55. Howell, G. A., Welch, M. G., and Frederickson, C. J. (1984) *Nature 308*, 736−738.
56. Lovell, M. A., Robertson, J. D., Teesdale, W. J., Campbell, J. L., and Markesbery, W. R. (1998) *J. Neurol. Sci. 158*, 47−52.
57. Atwood, C. S., Moir, R. D., Huang, X., Scarpa, R. C., Bacarra, M. E., Romano, D. M., Hartshorn, M. A., Tanzi, R. E., and Bush, A. I. (1998) *J. Biol. Chem. 273*, 12817−12826.
58. Johnstone, E. M., Chaney, M. O., Norris, F. H., Pascual, R., and Little, S. P. (1991) *Brain Res. Mol. Brain Res. 10*, 299−305.
59. Lansbury, P. T., Jr., Costa, P. R., Griffiths, J. M., Simon, E. J., Auger, M., Halverson, K. J., Kocisko, D. A., Hendsch, Z. S., Ashburn, T. T., and Spencer, R. G. (1995) *Nat. Struct. Biol. 2*, 990−998.
60. Lazo, N. D., and Downing, D. T. (1998) *Biochemistry 37*, 1731−1735.
61. Sunde, M., Serpell, L. C., Bartlam, M., Fraser, P. E., Pepys, M. B., and Blake, C. C. F. (1997) *J. Mol. Biol. 273*, 729−739.
62. Pike, C. J., Walencewicz, A. J., Glabe, C. G., and Cotman, C. W. (1991) *Brain Res. 563*, 311−314.
63. Pike, C. J., Walencewicz, A. J., Glabe, C. G., and Cotman, C. W. (1991) *Eur. J. Pharmacol. 207*, 367−368.
64. Pike, C. J., Burdick, D., Walencewicz, A. J., Glabe, C. G., and Cotman, C. W. (1993) *J. Neurosci. 13*, 1676−1687.
65. Simmons, L. K., May, P. C., Tomaselli, K. J., Rydel, R. E., Fuson, K. S., Brigham, E. F., Wright, S., Lieberburg, I., Becker, G. W., and Brems, D. N. (1993) *Mol. Pharmacol. 45*, 373−379.
66. Cribbs, D. H., Pike, C. J., Weinstein, S. L., Velazquez, P., and Cotman, C. W. (1997) *J. Biol. Chem. 272*, 7431−7436.
67. Hilbich, C., Kisters-Woike, B., Reed, J., Masters, C. L., and Beyreuthers, K. (1992) *J. Mol. Biol. 228*, 460−473.
68. Fraser, P. E., McLachlan, D. R., Surewicz, W. K., Mizzen, C. A., Snow, A. D., Nguyen, J. T., and Kirschner, D. A. (1994) *J. Mol. Biol. 244*, 64−73.
69. Boland, K., Manias, K., and Perlmutter, D. H. (1995) *J. Biol. Chem. 270*, 28022−28028.
70. Soto, C., Castaño, E. M., Frangione, B., and Inestrosa, N. C. (1995) *J. Biol. Chem. 270*, 3063−3067.
71. Esler, W. P., Stimson, E. R., Ghilardi, J. R., Lu Y. A., Felix, A. M., Vinters, H. V., Mantyh, P. W., Lee, J. P., and Maggio, J. E. (1996) *Biochemistry 35*, 13914−13921.
72. Wood, S. J., Wetzel, R., Martin, J. D., and Hurle, M. R. (1995) *Biochemistry 34*, 724−728.
73. Maggio, J. E., and Mantyh, P. W. (1996) *Brain Pathol. 6*, 147−162.
74. Manyth, P. W., Stimson, E. R., Ghilardi, J. R., Allen, C. J., Dahl, C. E., Whitcomb, D. C., Vigna, S. R., Vinters, H. V., Labenski, M. E., and Maggio, J. E. (1991) *Bull. Clin. Neurosci. 56*, 73−85.
75. Maggio, J. E., Stimson, E. R., Ghilardi, J. R., Allen, C. J., Dahl, C. E., Whitcomb, D. C., Vigna, S. R., Vinters, H. V., Labenski, M. E., and Mantyh, P. W. (1992) *Proc. Natl. Acad. Sci. U.S.A. 89*, 5462−5466.
76. Lee, J. P., Stimson, E. R., Ghilardi, J. R., Mantyh, P. W., Lu, Y. A., Felix, A. M., Llanos, W., Behbin, A., Cummings, M., Van Criekinge, M., et al. (1995) *Biochemistry 34*, 5191−5200.
77. Esler, W. P., Stimson, E. R., Ghilardi, J. R., Vinters, H. V., Lee, J. P., Mantyh, P. W., and Maggio, J. E. (1996) *Biochemistry 35*, 749−757.
78. Esler, W. P., Stimson, E. R., Ghilardi, J. R., Felix, A. M., Lu, Y. A., Vinters, H. V., Mantyh, P. W., and Maggio, J. E. (1997) *Nat. Biotechnol 15*, 258−263.
79. Wood, S. J., Maleef, B., Hart, T., and Wetzel, R. (1996) *J. Mol. Biol. 256*, 870−877.
80. Mehta, M. A., Gregory, D. M., Kiihne, S., Mitchell, D. J., Hatcher, M. E., Shiels, J. C., and Drobny, G. P. (1996) *Solid State Nucl. Magn. Reson. 7*, 211.

BI991527V